

**Differences in Chemoselectivity in Olefin Oxidation by a series of Non-porphyrin Manganese(IV)-oxo Complexes**

Journal:	<i>Dalton Transactions</i>
Manuscript ID	DT-ART-03-2022-000876
Article Type:	Paper
Date Submitted by the Author:	21-Mar-2022
Complete List of Authors:	Singh, Priya; University of Kansas College of Liberal Arts and Sciences, Chemistry Denler, Melissa; University of Kansas College of Liberal Arts and Sciences, Chemistry Mayfield, Jaycee; University of Kansas College of Liberal Arts and Sciences, Chemistry Jackson, Timothy; University of Kansas College of Liberal Arts and Sciences, Chemistry

Differences in Chemoselectivity in Olefin Oxidation by a series of Non-porphyrin Manganese(IV)–oxo Complexes

Priya Singh,^a Melissa C. Denler,^a Jaycee R. Mayfield,^a and Timothy A. Jackson^{*a}

*^aThe University of Kansas, Department of Chemistry and Center for Environmentally
Beneficial Catalysis, 1567 Irving Hill Road, Lawrence, KS 66045, USA.*

*To whom correspondence should be addressed:

Timothy A. Jackson

Phone: (785) 864-3968

taj@ku.edu

Abstract

High valent metal-oxo intermediates are versatile oxidants known to facilitate both oxygen atom transfer (OAT) and hydrogen atom transfer (HAT) reactions in nature. In addition to performing essential yet challenging biological reactions, these intermediates are known for their selectivity in favoring the formation of one oxidation product. To understand the basis for this selectivity, we explore the role of equatorial ligand field perturbations in Mn^{IV}-oxo complexes on chemoselectivity in cyclohexene oxidation. We also examine reactions of Mn^{IV}-oxo complexes with cyclohexene-*d*₁₀, cyclooctene, and styrene. Within this series, the product distribution in olefin oxidation is highly dependent on the coordination environment of the Mn^{IV}-oxo unit. While Mn^{IV}-oxo complexes with sterically encumbered, and slightly tilted, Mn=O units favor C=C epoxidation products in cyclohexene oxidation, a less encumbered analogue prefers to cleave allylic C–H bonds, resulting in cyclohexenol and cyclohexenone formation. These conclusions are drawn from GC–MS product analysis of the reaction mixture, changes in the UV-vis absorption spectra, and kinetic analyses. DFT computations establish a trend in thermodynamic properties of the Mn^{IV}-oxo complexes and their reactivity towards olefin oxidation on the basis of the Mn=O bond dissociation free energy (BDFE). The most reactive Mn^{IV}-oxo adduct from this series oxidizes cyclohexene-*d*₁₀, cyclooctene, and styrene to give corresponding epoxides as the only detected products. Collectively, these results suggest that the chemoselectivity obtained in oxidation of olefins is controlled by both the coordination environment around the Mn=O unit, which modulates the Mn=O BDFE, and the BDFEs of the allylic C–H bond of the olefins.

Introduction

Transition-metal catalysts are commonly used in the chemoselective and regioselective oxidation of saturated and unsaturated hydrocarbons.¹ Such reactions can result in the formation of asymmetric carbon centers and synthetically valuable intermediates, such as epoxides.^{1b, 1c} A range of 3d (Fe,² Co,³ Cr,⁴ and Mn⁵), 4d (Ru⁶, Pd,⁷ and Mo⁸) and 5d (Pt⁹) transition metal complexes have been used as catalysts for this purpose. Similar oxidation reactions with non-activated substrates are also performed by metalloenzymes, which utilize iron, manganese, and copper cofactors.¹⁰ These metalloenzymes often use molecular oxygen as oxidant and are able to perform substrate oxidation under mild conditions.¹¹ Therefore, there has been interest in designing more environmentally benign oxidation catalysts inspired by biology that use earth-abundant metals. Various Fe and Mn complexes supported by porphyrin¹² and salen^{5d, 13} scaffolds have been utilized as catalysts for the oxidation of unsaturated hydrocarbons yielding products with high efficiency and turnover.^{11c} Although porphyrin-based catalysts¹⁴ have been used for some time, there is significant recent work on non-porphyrin Fe and Mn systems, which are generally easier to access synthetically.¹⁵ One of the early biomimetic non-heme model complexes, [Fe(tpa)(CH₃CN)₂]²⁺ (tpa = tris(pyridylmethyl)amine), resembled non-heme oxygenases in terms of reactivity by catalyzing the oxidation of hydrocarbons.¹⁶ Over the years, a series of similar complexes have been synthesized and characterized to improve the oxidative properties of the complexes, increase the substrate scope, and understand the influence of catalyst structure on reaction rates and selectivity.^{15a}

Based on spectroscopic studies of a variety of metalloenzymes, high-valent metal-oxo intermediates initiate the difficult hydrocarbon oxidation step for several different types of enzymes.^{11c, 17} These observations have led model chemists to generate a range of metal-oxo complexes and investigate their reactivity. The past 15 years has witnessed remarkable progress in understanding the reactivity of metal-oxo complexes in initiating substrate oxidation by hydrogen atom transfer (HAT) and oxygen atom transfer (OAT) steps with a variety of hydrocarbons and olefins. Some of these complexes, and engineered cytochrome P450 models, have demonstrated regio- and chemoselectivity for rather challenging substrates such as olefins.^{11d, 15b, 18} To understand the basis for reaction selectivity, cyclohexene and cyclooctene have been used to probe metal-oxo preferences towards allylic oxidation (HAT) versus C=C epoxidation (OAT) reactions (Figure 1).¹⁹ From these studies, model complexes featuring metal-oxo moieties, such as [Ru^{IV}(O)(terpy)(bpm)]²⁺,²⁰

$[\text{Fe}^{\text{IV}}(\text{O})(\text{N4py})]^{2+}$, $[\text{Fe}^{\text{IV}}(\text{O})(\text{Bn-TPEN})]^{2+}$,²¹ and the manganese complexes $[\text{Mn}^{\text{IV}}(\text{O})(\text{N4py})]^{2+}$ and $[\text{Mn}^{\text{IV}}(\text{O})(\text{Bn-TPEN})]^{2+}$,²² have shown a strong preference for allylic oxidation over epoxidation. In contrast, $\text{Fe}^{\text{IV}}\text{-oxo}$ and $\text{Mn}^{\text{IV}}\text{-oxo}$ intermediates, supported by similar N_4 and N_5 ligands, have been proposed in olefin epoxidation reactions (rather than allylic C–H bond oxidation) under catalytic conditions.^{15b, 18a-c, 23} These observations raise several questions. What factors influence chemoselectivity in olefin oxidation by metal-oxo complexes? Why do isolable metal-oxo model complexes favor allylic oxidation over olefin epoxidation? At present, these questions are only partially answered. Chemoselectivity in olefin oxidation has been shown to be influenced by a host of factors, including temperature,^{12c} equatorial ligand-field strength,²⁴ spin inversion probabilities²¹ and hydrogen atom tunneling,²¹ the identity of the axial ligand trans to the oxo group,^{18d} and the presence of Brønsted acids.²²

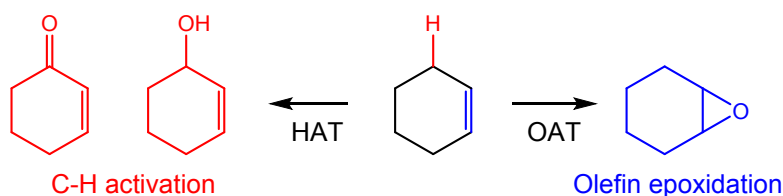


Figure 1. Oxidation products of cyclohexene via HAT (C – H hydroxylation) and OAT (C=C epoxidation).

Previously our group reported a series of $\text{Mn}^{\text{IV}}\text{-oxo}$ species bound to neutral pentadentate derivatives of the N4py scaffold.²⁵ These N_5 ligands differ in electronic and steric properties by virtue of substitution of two pyridyl groups with quinolinyl (N2py2Q), benzimidazolyl (N2py2B), or 3,4-dimethyl-5-methoxypyridyl ($^{\text{DMM}}\text{N4py}$) moieties (Figure 2).²⁵ We probed the reactivities of $[\text{Mn}^{\text{IV}}(\text{O})(\text{N4py})]^{2+}$ (**1**), $[\text{Mn}^{\text{IV}}(\text{O})(\text{N2py2Q})]^{2+}$ (**2**), $[\text{Mn}^{\text{IV}}(\text{O})(\text{N2py2B})]^{2+}$ (**3**), and $[\text{Mn}^{\text{IV}}(\text{O})(^{\text{DMM}}\text{N4py})]^{2+}$ (**4**) with substrates with strong C–H bonds^{25b, 26} (e.g. cyclohexane, toluene, and ethylbenzene), and demonstrated that such reactions follow a HAT mechanism. We also examined OAT reactions of these $\text{Mn}^{\text{IV}}\text{-oxo}$ complexes with thioanisole and its derivatives.^{25a, 27} For both HAT and OAT reactions, the reactivity of **2** was the fastest in this series. The HAT reactions of **2** showed a ~ 70 -fold enhancement in rate compared to **4**, while the OAT reactions of **2** in thioanisole sulfoxidation showed an enhancement of 4000-fold when compared to **4**. This large rate variation in the reactivity was attributed to the elongated Mn–N(quinolinyl) distances of **2**, which makes this Mn center most electron deficient.

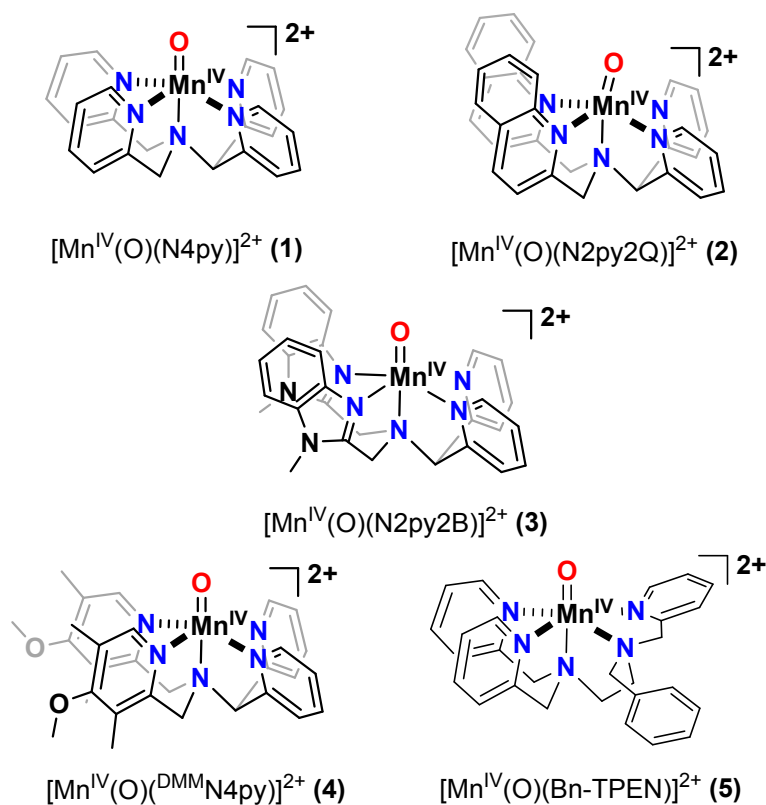


Figure 2. Structures of Mn^{IV}-oxo complexes considered in this work

While **2** was the fastest oxidant regardless of the reaction (HAT or OAT), complexes **3** and **4** showed an inversion in ordering depending on the reaction type. For HAT reactions with hydrocarbons, **4** showed a rate 1.3-fold greater than that of **3**, while for an OAT reaction (thioanisole oxidation), **3** was 12-fold faster than **4**. The experimental reaction rates thus led to the order of $2 > 1 > 4 > 3$ for HAT reactions and $2 > 1 > 3 > 4$ in OAT reactions. Given the differences in HAT and OAT reactions in this series, we envisaged that these equatorial ligand field perturbations in complexes **2-4** might show different preferences for allylic C–H bond oxidation versus C=C bond epoxidation in olefin oxidation. In this current work, we determined the utility of the Mn^{IV}-oxo adducts **2-4** in oxidizing several olefins (styrene, cyclohexene, and cyclooctene). We have found that non-porphyrin Mn^{IV}-oxo adducts with bulky substituents around the Mn=O unit prefer C=C epoxidation over C–H hydroxylation. These observations follow the prior trends of HAT and OAT ordering for these complexes. We also demonstrate here that these reactivity trends can be rationalized by considering the Mn^{IV}=O and Mn^{III}O–H bond dissociation free energy (BDFEs), which pertain to the thermodynamic driving force for OAT and HAT reactions, respectively. Moreover, the reaction chemoselectivity of allylic oxidation versus epoxidation is dependent on the substrate C–H bond strength, as demonstrated by the oxidation of cyclohexene-d₁₀,

cyclooctene, and styrene, which predominantly yielded epoxidation products. These results provide valuable information on factors affecting chemoselectivity of the olefin epoxidation reactions by high-valent Mn-oxo species and show that variations in reactivity among similar complexes can be rationalized on the basis of reaction thermodynamics.

Experimental Methods

Materials and Instrumentation. All solvents and chemicals were purchased from commercial vendors and used without further purification unless otherwise described. Iodosobenzene (PhIO) was prepared from iodosobenzene diacetate following a published procedure.²⁸ All kinetic experiments were performed by electronic absorption spectroscopy. Electronic absorption data were collected on either an Agilent 8453 or Cary 50 Bio spectrometer. Temperature control was achieved using either a Unisoku (USP-203-A) cryostat or a Quantum Northwest cryostat (t2 Sport). Gas chromatography–mass spectrometry data, used for product analysis, were collected on a Quattro Micro GC quadrupole mass analyzer via an Agilent 6890 N gas chromatograph. A 5% phenyl methyl silicone stationary phase (HP-5 MS) 12 m column was used with a helium carrier gas with a flow rate of 2 mL min⁻¹. The injector port was heated to 240 °C, and 1 μL of sample was injected with a split ratio of 20:1. The GC thermal gradient was an initial 50 °C which was held for 1 min before increasing 50 °C min⁻¹ to 300 °C and held for 2 min.

Synthesis and Characterization. The N2py2Q, N2py2B and ^{DMM}N4py ligands and the corresponding Mn^{II} species were synthesized according to previously published methods.^{25a, 25b, 29} [Mn^{IV}(O)(N2py2Q)]²⁺ (**2**), [Mn^{IV}(O)(N2py2B)]²⁺ (**3**) and [Mn^{IV}(O)(^{DMM}N4py)]²⁺ (**4**) were all prepared *in situ* by reacting the corresponding Mn^{II} species with 10, 2.5, and 1.2 equiv. of iodosobenzene (PhIO), respectively, in 2,2,2-trifluoroethanol (TFE) at 25°C. The amounts of PhIO used in these reactions were based on previous studies that demonstrated maximal yield of the Mn^{IV}-oxo complexes under these conditions.^{25a, 25b, 29}

Oxidation of Cyclohexene by Mn^{IV}-oxo adducts. To a 1.0 mM solution of **2** in TFE, varying amounts of cyclohexene (0.01 M–0.04 M) dissolved in 100 μL of acetonitrile (MeCN) were added. The addition of cyclohexene led to the disappearance of the near-IR absorption feature at 1020 nm for **2**. The corresponding decay in absorbance over time was fit according to a pseudo-first-order model to obtain an observed rate constant (k_{obs}). Each reaction was repeated in triplicate. A linear dependence of k_{obs} on the concentration of cyclohexene was observed, which allowed determination of a second order rate constant (k_2)

for the oxidation of cyclohexene by **2**. Because of concerns regarding a reaction between **2** and MeCN, kinetic experiments for **2** were repeated with cyclohexene dissolved in CH₂Cl₂, which yielded a similar k_2 value (Figure S1). Additionally, a k_{obs} value was determined for the addition of 200 μL MeCN (~ 1740 equiv.) to **2** (Figure S2). Oxidation reactions of cyclohexene with complexes **3** and **4** were also explored, and kinetic data were obtained using a similar procedure with the only difference being in the concentrations of cyclohexene used (0.1 M–0.5 M). The challenges related to solubility at 0.2 M and higher concentrations of cyclohexene were resolved by dissolving the substrate in 200 μL CH₂Cl₂. Following the reaction of Mn^{IV}-oxo adducts with 50 equiv. cyclohexene, the reaction solution was passed through a silica plug and the eluate was analyzed by GC–MS to identify the organic products.

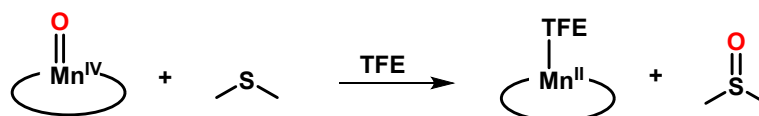
Reactivity of Mn^{IV}-oxo species with other olefins. To a 1.0 mM solution of **2** in TFE at 25°C, varying amounts of excess substrate (cyclohexene-d₁₀, styrene, and cyclooctene) were added. Substrate concentrations were as follows: cyclohexene-d₁₀ in TFE (0.01 M–0.04 M), styrene in TFE (0.04 M–0.1 M), and cyclooctene in CH₂Cl₂ (0.03 M–0.08 M). The decay of the corresponding Mn^{IV}-oxo species, as evident from the near-IR absorption feature, was monitored and the resulting time trace was fit to a pseudo-first order model. For the reactions of **2** with cyclohexene-d₁₀, styrene, and cyclooctene, plots of k_{obs} versus substrate concentration were linear, and a fit yielded k_2 values. Attempts were made to assess the reactivity of **3** and **4** with respect to cyclohexene-d₁₀, styrene, and cyclooctene under similar conditions. Unfortunately, the reactions were too slow, even at 0.2 M concentration of substrates, to obtain any reasonable data.

Product analysis. A reaction between 1.6 mg (0.002 mmol) [Mn^{II}(OTf)(N₂py₂Q)]⁺ and 4.4 mg (0.020 mmol) PhIO in 2.0 mL TFE formed **2** in 3 minutes under an inert atmosphere. To this solution, 10 μL (0.099 mmol) of cyclohexene was added directly and stirred. The electronic absorption band at 1020 nm decayed by pseudo first-order kinetics over a period of 15 minutes. After completion of the reaction, the solution was passed through silica and diluted with ethyl acetate in a 10.0 mL volumetric flask. The eluate was further diluted to appropriate concentration and an internal standard (naphthalene) of known concentration was added to the sample. A similar procedure was used to prepare GC–MS samples for reactions of cyclohexene oxidation using **3** and **4**. A standard calibration curve was made by using known concentrations of authentic samples. A quantitative analysis of the oxidation products was obtained by comparing the peak areas of the analytes with that of standards by using naphthalene as an internal standard. Due to complications in analyzing the

GC–MS data, the product formed during oxidation of cyclohexene-d₁₀ was analyzed using ²H-NMR. For ²H-NMR analysis, a 10 mM solution of **2** was reacted with 20 equiv. cyclohexene-d₁₀ (~25 μL) in 1.0 mL TFE for 20 minutes. The reaction solution was then passed through a silica plug and diluted to 2.0 mL with ethyl acetate. Approximately 0.6 mL of this stock solution were taken in an NMR tube along with CDCl₃ (6 μL of 30% solution in ethyl acetate) as an external reference ($\delta = 7.2$ ppm). The peaks corresponding to cyclohexene-d₁₀ and cyclohexene oxide-d₁₀ were observed and compared to that previously reported.³⁰ The product obtained for the reaction of **2** with cyclooctene and styrene were also analyzed using GC–MS, and their identity was confirmed by comparison with authentic samples.

Computational details. All density functional theory (DFT) calculations were performed using the ORCA 4.2.1 software package.³¹ Gas-phase geometry optimizations of all species were performed with B3LYP³² functional using Grimme's D3³³ dispersion correction with the Becke-Johnson damping scheme.³⁴ A larger basis set, def2-TZVP, was employed for heavy atoms such as Mn, N, and O, while def2-SVP was used for C and H.³⁵ To speed up the calculations, the RIJCOSX approximation was used in combination with the automatic auxiliary basis set feature (AutoAux).³⁶ Analytical frequency calculations were performed at the same level of theory and basis sets as geometry optimizations. All species were verified to be minima on the potential energy surface by having no imaginary frequencies. Single-point energy calculations were performed to determine electronic energies for all structures using the B3LYP-D3 functional and the def2-TZVPP basis set for all atoms. Zero-point correction to the energies, as well as rotational, translational, and vibrational entropies, were obtained from the analytical frequency calculations. Enthalpies were taken as the sum of the electronic energy (from single-point calculations) and the zero-point energy, and free energies were determined by combining enthalpy and entropy terms. For calculations used in determination of BDFE of Mn^{III}O-H species, all single point energy calculations were performed with the solvent model.³⁷ In order to validate the accuracy of single point energies determined from gas phase structures, **1** was optimized with and without a solvent model. Frequency calculations confirmed that both structures were at a true minimum. The difference in single point energy for the structures of **1** optimized in the gas phase and that with the solvent model was only 0.96 kcal mol⁻¹. Since the energy difference is smaller than the expected accuracy of DFT-computed energies, we determined that the use of structures optimized in the gas phase would result in no substantive change to the DFT results.

To determine the Mn=O BDFE values for each Mn^{IV}=O complex, an oxygen-atom transfer reaction with dimethyl sulfide was considered (Scheme 1). The free energy of the reaction (ΔG_{DFT}) was calculated using equation 1, using DFT-derived values of free energies of the Mn^{IV}-oxo complex, dimethyl sulfide (DMS), TFE, the Mn^{II} complex (TFE bound), and dimethyl sulfoxide (DMSO) (see SI for details). The calculated value of ΔG_{DFT} , along with the BDE value of 87 kcal mol⁻¹ reported for dimethyl sulfoxide (DMSO),³⁸ was used to calculate the Mn=O BDFEs of the Mn^{IV}=O complexes using equation 2. As noted by Holm *et al.*, as the entropic contributions to the BDE for DMSO are negligible, it is safe to assume that $\text{BDE}_{\text{DMSO}} \approx \text{BDFE}_{\text{DMSO}}$.

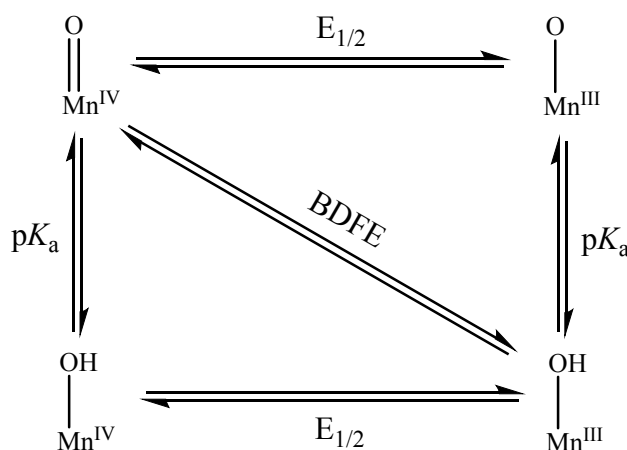


Scheme 1. Reaction between Mn^{IV}-oxo complexes and dimethyl sulfide.

$$\Delta G_{\text{DFT}} = [G_{\text{DMSO}} + G_{\text{TFE}}] - [G_{\text{DMS}} + G_{\text{Mn}^{\text{IV}}\text{L}}^{\text{O}} + G_{\text{TFE}}] \quad \text{Equation 1}$$

$$\Delta G_{\text{DFT}} = \Delta G_{\text{DMSO/DMS}} + \Delta G_{\text{Mn}^{\text{IV}}\text{L}/\text{Mn}^{\text{II}}\text{L}}^{\text{O/TFE}} \quad \text{Equation 2}$$

We used the Bordwell equation (equation 3) to obtain O–H BDFEs for Mn^{III}-hydroxo complexes (Mn^{III}O–H bond), which are products of HAT reactions with Mn^{IV}-oxo species (Scheme 2). The equation is comprised of the reduction potential of the Mn^{IV/III} couple for **1–4** ($E_{1/2}$) and the pK_{a} of the corresponding Mn^{III}-OH species, both of which were determined by DFT calculations (see SI for further details).

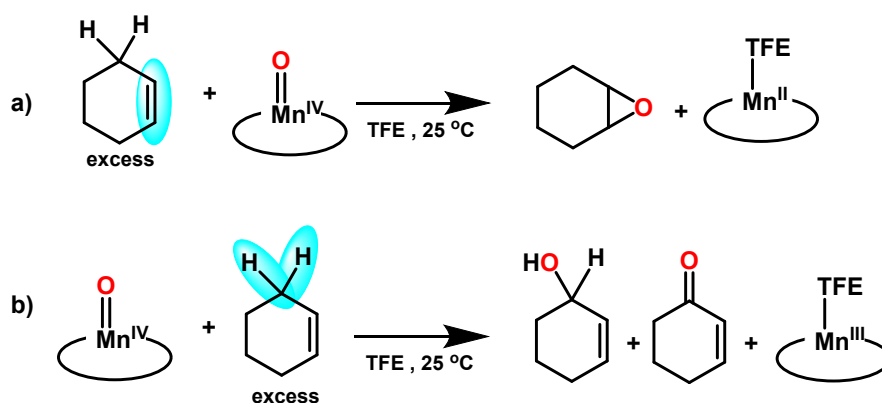


Scheme 2. Square plot depicting how the BDFE of a Mn^{III}-hydroxo complex (diagonal) can be described in terms of stepwise reduction and protonation steps (edges).

$$\text{BDFE} = 23.06E_{1/2} + 1.37 pK_{\text{a}} + C_G \quad \text{Equation 3}$$

Results and Discussion

Reactivity of Mn^{IV}-oxo adducts with cyclohexene. To probe the propensity of the Mn^{IV}-oxo species **2-4** in olefin oxidation, we first investigated the reactions of these complexes with cyclohexene. This substrate is informative, as it can undergo epoxidation to give cyclohexene oxide or allylic oxidation to give the corresponding alcohol and/or ketone products (Scheme 3). Upon the addition of varied amounts of cyclohexene (dissolved in MeCN) to a 1.0 mM solution of **2**, the near-IR absorption feature at 1020 nm decayed, following pseudo first-order kinetics (Figure 3). Interestingly, as the 1020 nm signal decayed, a new band formed at 620 nm. The formation of a band at 620 nm was previously observed in the reaction of **2** with hydrocarbons and was taken to mark the formation of a mononuclear Mn^{III} product.^{25b} The rate of formation of this new species at 620 nm ($k_{\text{obs}} = 2.0(1) \times 10^{-2} \text{ s}^{-1}$) is similar to the decay rate of the feature at 1020 nm ($k_{\text{obs}} = 2.4(2) \times 10^{-2} \text{ s}^{-1}$; see Figure 3), suggesting that the disappearance of the Mn^{IV}-oxo adduct is related to the appearance of the Mn^{III} product. A Mn^{III} complex is a potential product of allylic oxidation of cyclohexene by **2**. The abstraction of a hydrogen atom from the alkene C–H bond results in the formation of a Mn^{III}-OH species and a carbon-centered radical that interact weakly forming a cage compound. These weakly interacting products can undergo a rebound reaction to form a Mn^{II} species and hydroxylated product. Alternatively, the substrate radical can diffuse from the cage and react with O₂ to give a Mn^{III} product and hydroxylated products. The latter, non-rebound pathway has been the most common mode of C–H bond oxidation by Mn^{IV}-oxo complexes.³⁹ In contrast, epoxidation of cyclohexene by an OAT mechanism should yield a Mn^{II} product that would not contribute absorption bands in the visible region (Scheme 3). Thus, the formation of the 620 nm band during the reaction of **2** and cyclohexene seems to imply that the allylic oxidation pathway occurs to some extent.



Scheme 3. Cyclohexene oxidation by Mn^{IV}-oxo complexes showing a) epoxidation products and b) allylic oxidation products.

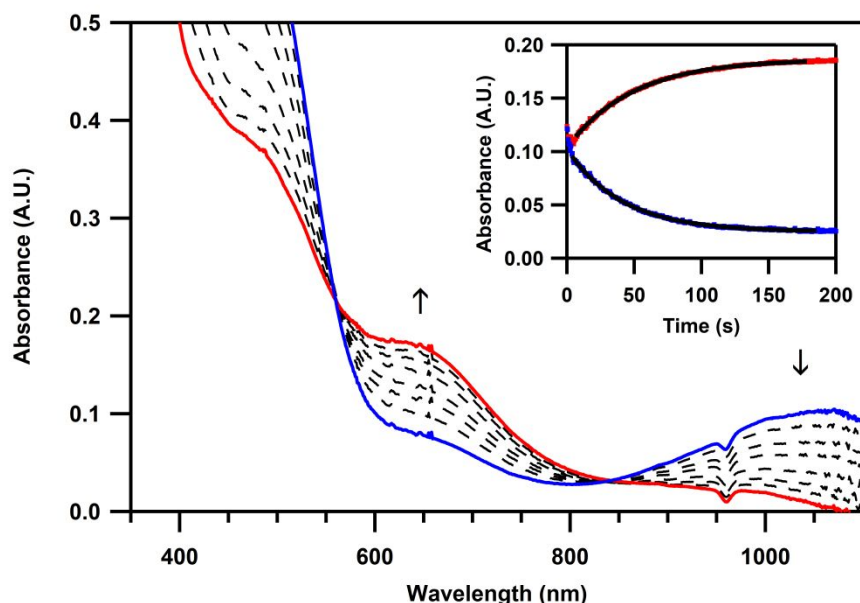


Figure 3. Reaction of 1.0 mM $[\text{Mn}^{\text{IV}}(\text{O})(\text{N}2\text{py}2\text{Q})]^{2+}$ (**2**) with 40 equiv. cyclohexene in TFE (cyclohexene dissolved in MeCN). Inset: decay of the feature at 1020 nm ($k_{\text{obs}} = 2.4(2) \times 10^{-2} \text{ s}^{-1}$) and the growth of the feature at 620 nm ($k_{\text{obs}} = 2.0(1) \times 10^{-2} \text{ s}^{-1}$).

The corresponding pseudo first-order rate constant (k_{obs}) for the decay of **2** in the presence of cyclohexene showed a linear increase with increasing cyclohexene concentration. A linear fit to these data yielded a second-order rate constant (k_2) of $4.6(1) \times 10^{-1} \text{ M}^{-1} \text{ s}^{-1}$ at 298 K in TFE⁴⁰ (Figure 4, orange circles). This rate is 11 and 3-fold faster than the cyclohexene oxidation rates obtained for **1** and **5**, respectively (Figure 5, Table 1).

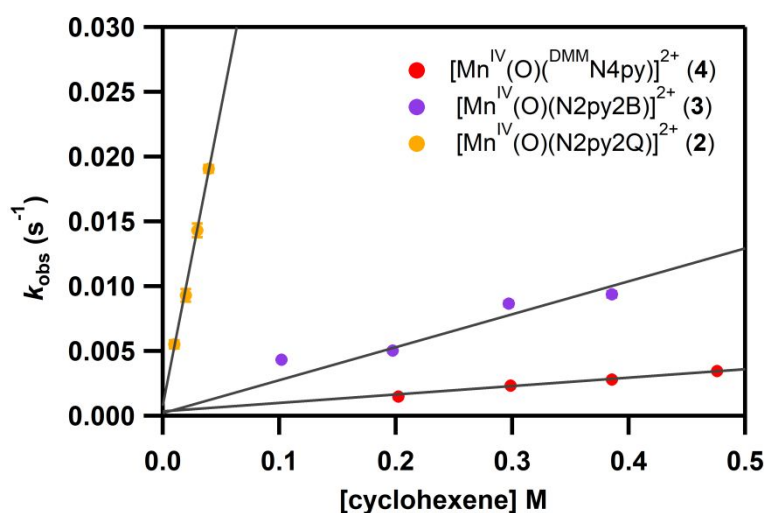
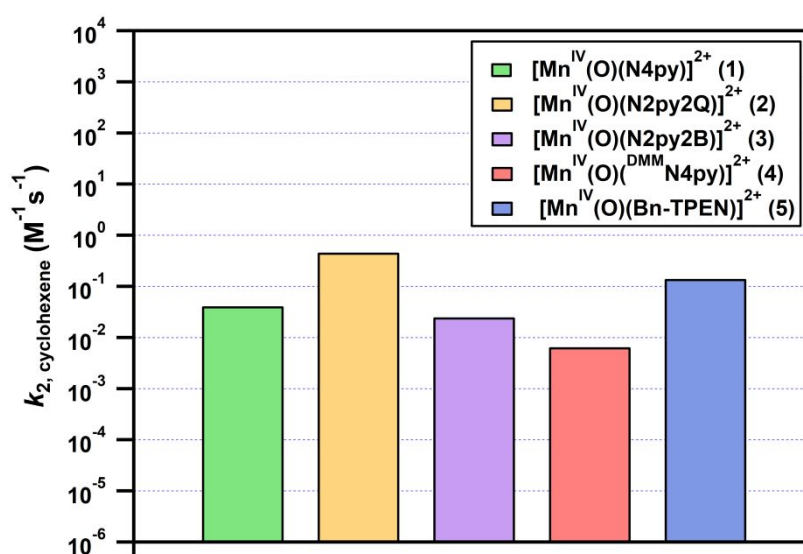


Figure 4. Plots of the pseudo-first-order rate constants (k_{obs}) against cyclohexene concentration for the oxidation reactions of cyclohexene with $[\text{Mn}^{\text{IV}}(\text{O})(\text{N}2\text{py}2\text{Q})]^{2+}$ (**2**) (orange circles), $[\text{Mn}^{\text{IV}}(\text{O})(\text{N}2\text{py}2\text{B})]^{2+}$ (**3**) (purple circles) and $[\text{Mn}^{\text{IV}}(\text{O})(\text{DMMN}4\text{py})]^{2+}$ (**4**) (red circles) in TFE for substrate dissolved in MeCN.

Table 1. Second-order rate constants for oxidation of olefins by Mn^{IV}-oxo adducts in TFE at 298 K.

Complex	k_2 (M ⁻¹ s ⁻¹)			
	cyclohexene	cyclohexene-d ₁₀	cyclooctene	styrene
[Mn ^{IV} (O)(N2py2Q)] ²⁺ (2)	4.6(1) × 10 ⁻¹	1.6(1) × 10 ⁻¹	6(1) × 10 ⁻¹	7(1) × 10 ⁻¹
[Mn ^{IV} (O)(N2py2B)] ²⁺ (3)	2.5(1) × 10 ⁻²	–	–	–
[Mn ^{IV} (O)(^{DMM} N4py)] ²⁺ (4)	6.5(1) × 10 ⁻³	–	–	–
[Mn ^{IV} (O)(N4py)] ²⁺ ^a (1)	4.1(2) × 10 ⁻²	4.4(2) × 10 ⁻³	5.4(3) × 10 ⁻³	3.3(2) × 10 ⁻⁴ ^b
[Mn ^{IV} (O)(Bn-TPEN)] ²⁺ ^a (5)	1.4(1) × 10 ⁻¹	4.3(2) × 10 ⁻²	3.3(2) × 10 ⁻²	–

^aThe data have been taken from previously reported values (see reference 22b). ^bThis reaction was performed in a mixture of TFE–MeCN at 273 K.⁴¹

**Figure 5.** Comparison of second order rate constants of cyclohexene oxidation by Mn^{IV}-oxo species at 298 K. Data for **1** and **5** are taken from reference 22b.

Similarly, the addition of excess cyclohexene (0.1–0.4 mM) to a solution of **3** in TFE causes the absorption band of the Mn^{IV}-oxo complex at 940 nm to decay following first-order kinetics (Figure 6). In this case, there is only a minimal growth of a feature at 620 nm, which is associated with the formation of a small amount of Mn^{III} product. In addition, the rate of formation of the 620 nm band is slower than the decay of the 940 nm signal (Figure 6, inset). These results could suggest a preference for two-electron OAT, resulting in Mn^{II} and epoxide products (Scheme 1). The second-order rate constant obtained for cyclohexene oxidation by **3** (Figure 4, purple circles) is 2.5(3) × 10⁻² M⁻¹ s⁻¹, which is 18-fold slower than that of **2** but comparable to that of **1** (Figure 5). We also probed the reactivity of **4** with cyclohexene under similar reaction conditions. Upon addition of excess cyclohexene (0.2–0.5 mM), the absorption band at 920 nm corresponding to the Mn^{IV}-oxo species disappeared with

concomitant growth of a Mn^{III} feature at 600 nm (Figure 7). This latter band was metastable and showed a slow decay. The rate of formation of this intermediate is similar to the rate of decay of **4** (Figure 7, inset), suggesting concomitant formation of the Mn^{III} product with decay of the Mn^{IV}-oxo adduct. A second-order rate constant (k_2) of $6.5(5) \times 10^{-3} \text{ M}^{-1} \text{ s}^{-1}$ at 298 K was determined for the oxidation of cyclohexene by **4**. The k_2 obtained for **4** is 70-fold slower than that of **2** and 4-fold slower than that of **3** (Figure 5). This observed trend in k_2 ($\mathbf{2} > \mathbf{1} > \mathbf{3} > \mathbf{4}$) for cyclohexene oxidation is similar to the trend in rates for thioanisole sulfoxidation.^{25a}

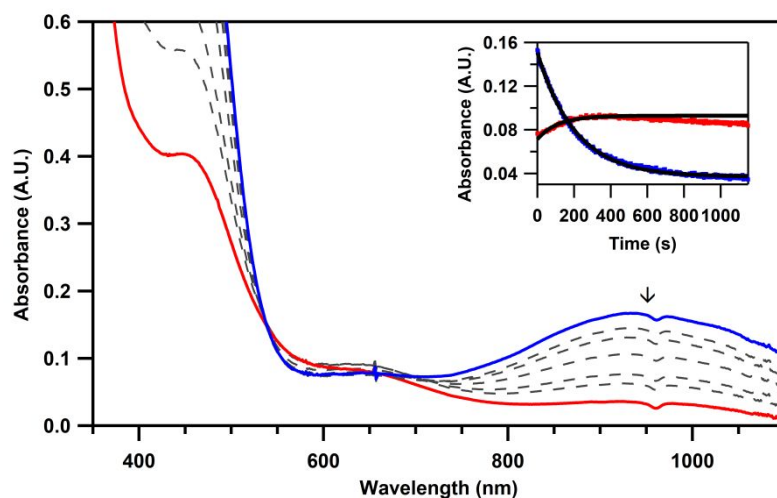


Figure 6. Reaction of 1.0 mM $[\text{Mn}^{\text{IV}}(\text{O})(\text{N}2\text{py}2\text{B})]^{2+}$ (**3**) with 200 equiv. cyclohexene in TFE (cyclohexene dissolved in MeCN). Inset: decay of the feature at 940 nm ($k_{\text{obs}} = 4.9(3) \times 10^{-3} \text{ s}^{-1}$) and the growth of the feature at 620 nm ($k_{\text{obs}} = 7.9(3) \times 10^{-3} \text{ s}^{-1}$).

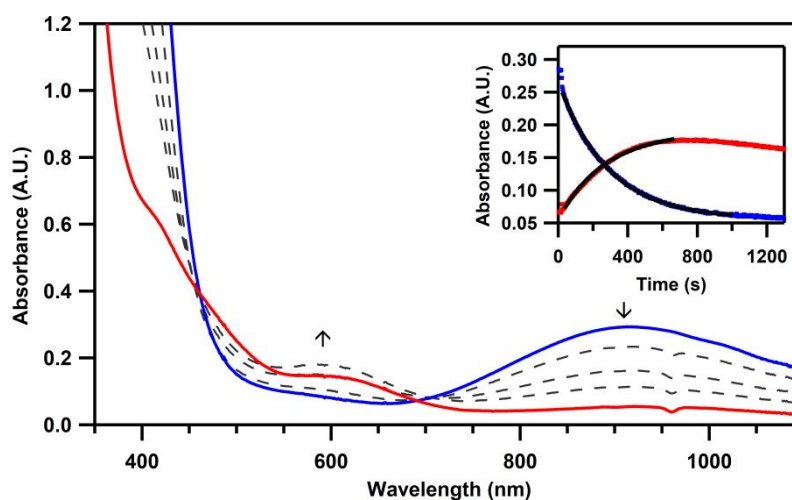


Figure 7. Reaction of 1.0 mM $[\text{Mn}^{\text{IV}}(\text{O})(\text{DMN}4\text{py})]^{2+}$ (**4**) with 400 equiv. cyclohexene in TFE (cyclohexene dissolved in MeCN). Inset: decay of the feature at 920 nm ($k_{\text{obs}} = 3.5(2) \times 10^{-3} \text{ s}^{-1}$) and the growth of the feature at 620 nm ($k_{\text{obs}} = 3.9(5) \times 10^{-3} \text{ s}^{-1}$).

Chemoselectivity in cyclohexene oxidation by Mn^{IV}-oxo adducts. The organic products formed from the reactions of Mn^{IV}-oxo complexes **2-4** with excess cyclohexene

were identified by GC, and quantitative analyses were performed by the GC–MS technique. For cyclohexene oxidation by **2**, the quantitative analysis yields 60% cyclohexene oxide and 17% of both cyclohexenol and cyclohexenone (Figure 8) relative to the oxidant **2**. This distribution in products reveals a roughly 2:1 preference for epoxidation over allylic oxidation by **2** (Table 2). Cyclohexene oxidation by **3** also yields a near 2:1 ratio of epoxidation over allylic oxidation, with a yield of 41% for cyclohexene epoxide and 11% for both cyclohexenol and cyclohexenone (Figure 8 and Table 2). In contrast, the oxidation of cyclohexene by **4** gave a 35% yield of cyclohexenol, a 12% yield of cyclohexenone, and a 21% yield of epoxide. Thus, **4** shows a preference for C–H bond oxidation, with an epoxidation to allylic oxidation ratio of 0.4:1 (Figure 8). Collectively, these results reveal that **4**, which has the slowest rate of reaction with cyclohexene, reacts predominantly by abstracting an allylic hydrogen atom to preferentially form cyclohexenone and cyclohexenol, while the more reactive complexes **2** and **3** prefer OAT to the C=C double bond of cyclohexene. The chemoselectivity observed in cyclohexene oxidation by **2** and **3** is also in stark contrast with that reported for $[\text{Mn}^{\text{IV}}(\text{O})(\text{N}4\text{py})]^{2+}$ (**1**) and $[\text{Mn}^{\text{IV}}(\text{O})(\text{Bn-TPEN})]^{2+}$ (**5**). For those complexes allylic oxidation was favored over epoxidation, with selectivity epoxide: allylic oxidation product ratios of 0.2:1 and 0.5:1, respectively (Table 2).²² To the best of our knowledge, **2** and **3** are the first Mn^{IV} -oxo complexes to prefer olefin epoxidation over allylic oxidation.

Table 2. Summary of product analysis for oxidation of cyclohexene by Mn^{IV} -oxo adducts in TFE at 298 K.

Complex	Product Yield (%)			
	cyclohexene reaction			
	epoxide	ketone	alcohol	Selectivity ^a
$[\text{Mn}^{\text{IV}}(\text{O})(\text{N}2\text{py}2\text{Q})]^{2+}$ (2)	60	17	17	1.8
$[\text{Mn}^{\text{IV}}(\text{O})(\text{N}2\text{py}2\text{B})]^{2+}$ (3)	41	11	11	1.9
$[\text{Mn}^{\text{IV}}(\text{O})(\text{DMMN}4\text{py})]^{2+}$ (4)	21	12	35	0.4
$[\text{Mn}^{\text{IV}}(\text{O})(\text{N}4\text{py})]^{2+}$ (1) ^b	6	6	34	0.2
$[\text{Mn}^{\text{IV}}(\text{O})(\text{Bn-TPEN})]^{2+}$ (5) ^b	18	8	26	0.5

^a Selectivity is calculated as the ratio of epoxide (cyclohexene oxide) to allylic oxidation products (cyclohexenol and cyclohexenone). ^b Experimental data are taken from reference 22b.

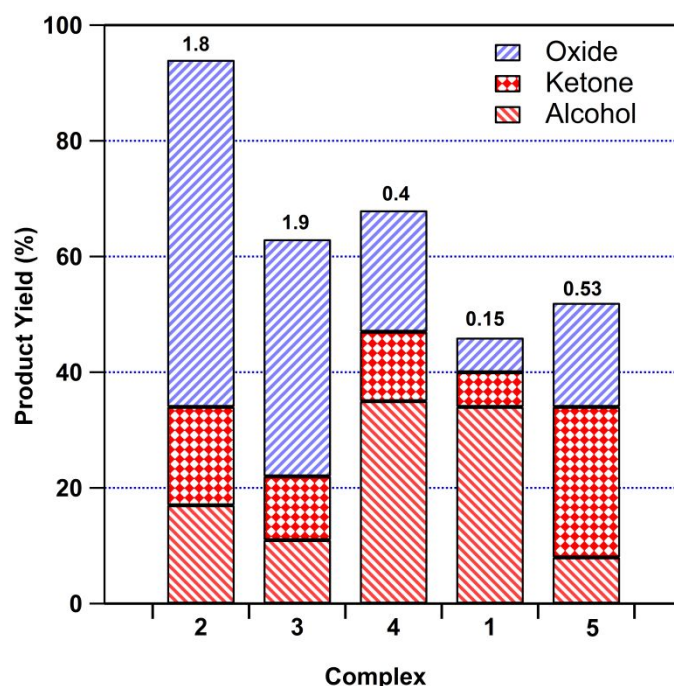


Figure 8. Summary of chemoselectivity observed for the oxidation of cyclohexene by Mn^{IV}-oxo adducts in TFE at 298 K. The numbers at the top of each bar represent the ratio of epoxidation to allylic oxidation. Data for **1** and **5** are taken from previous literature.²²

Oxidation of cyclohexene-*d*₁₀ by Mn^{IV}-oxo adducts. To further examine cyclohexene oxidation by **2**, we utilized cyclohexene-*d*₁₀ as a substrate. From prior work, C–H bond oxidation by **2** showed a large H/D kinetic isotope effect of 5.3 (where $\text{KIE} = k_{2(\text{H})}/k_{2(\text{D})}$). Therefore, the use of cyclohexene-*d*₁₀ should suppress the allylic oxidation rate while the epoxidation rate should be unaffected. A comparison of rates of cyclohexene and cyclohexene-*d*₁₀ would thus yield an apparent KIE ($\text{KIE}_{\text{app}} = k_2(\text{cyclohexene})/k_2(\text{cyclohexene-}d_{10})$). This KIE is apparent in the sense that $k_2(\text{cyclohexene})$ represents a blended rate with contributions from both allylic oxidation and epoxidation, while $k_2(\text{cyclohexene-}d_{10})$ should be largely the rate of epoxidation. Under these assumptions a large KIE_{app} would reflect a dominant allylic oxidation mechanism for cyclohexene oxidation, while a KIE_{app} close to 1 would be expected when OAT is dominant.

Addition of cyclohexene-*d*₁₀ (0.01–0.04 M) to a solution of **2** led to decay of the near IR absorption band at 1020 nm (Figure S3). Notably, with the decay of the absorption band at 1020 nm there is still formation of a mononuclear Mn^{III} species, as evident from the growth of the 620 nm absorption band (Figure S3). However, the formation of this Mn^{III} intermediate is slower than the decay rate of the Mn^{IV}-oxo adduct by a factor of 2 (Figure S3, inset). The second-order rate constant (k_2) of $1.6(1) \times 10^{-1} \text{ M}^{-1} \text{ s}^{-1}$ for oxidation of cyclohexene-*d*₁₀ was slower than the rate for cyclohexene oxidation (Figure 9), giving a KIE_{app} of 2.9. This value

is less than that observed for HAT reactions of **2** ($\text{KIE} \approx 5$).^{25b, 26} An analysis of the organic products of cyclohexene- d_{10} oxidation by **2** using ^2H -NMR showed formation of cyclohexene oxide- d_{10} as the sole detected product (Figure S4). Prior studies of cyclohexene- d_{10} oxidation by **5** and **1** in TFE-MeCN at 298 K yielded KIE_{app} values of 3.3 and 9.3.²² In those cases the larger KIE_{app} values are in accordance with the preference for allylic oxidation over epoxidation.

As the product analysis for cyclohexene- d_{10} oxidation by **2** does not reveal any allylic oxidation products, the appearance of the Mn^{III} product in the UV-vis spectrum is unexpected. Since **2** is a strong oxidant, we hypothesized that **2** can undergo comproportionation with $[\text{Mn}^{\text{II}}(\text{OTf})(\text{N}2\text{py}2\text{Q})]^+$, which is produced after cyclohexene- d_{10} oxidation, to yield the Mn^{III} product (Scheme 4). To test this hypothesis, a 1.0 mM solution of **2** was formed using 2 equiv. PhIO in TFE at 298 K, and 1.0 equiv. $[\text{Mn}^{\text{II}}(\text{OTf})(\text{N}2\text{py}2\text{Q})]^+$ was added to **2** (a smaller excess of PhIO was used in this reaction to minimize any reaction between PhIO and the added Mn^{II} complex). In this reaction, the near-IR absorption band at 1020 nm, corresponding to **2**, decayed with the growth of a feature at 620 nm (Figure S5). The rate of this comproportionation reaction ($k_{\text{obs}} = 1.1(3) \times 10^{-3} \text{ s}^{-1}$) resulting in formation of Mn^{III} intermediate is comparable to the rate of formation of the Mn^{III} species in cyclohexene- d_{10} oxidation ($k_{\text{obs}} = 4.7(2) \times 10^{-3} \text{ s}^{-1}$), lending credence to the comproportionation hypothesis. Moreover, the relatively slow rate of reaction of cyclohexene- d_{10} with **2** allows the comproportionation reaction between **2** and $[\text{Mn}^{\text{II}}(\text{OTf})(\text{N}2\text{py}2\text{Q})]^+$ to be competitive.

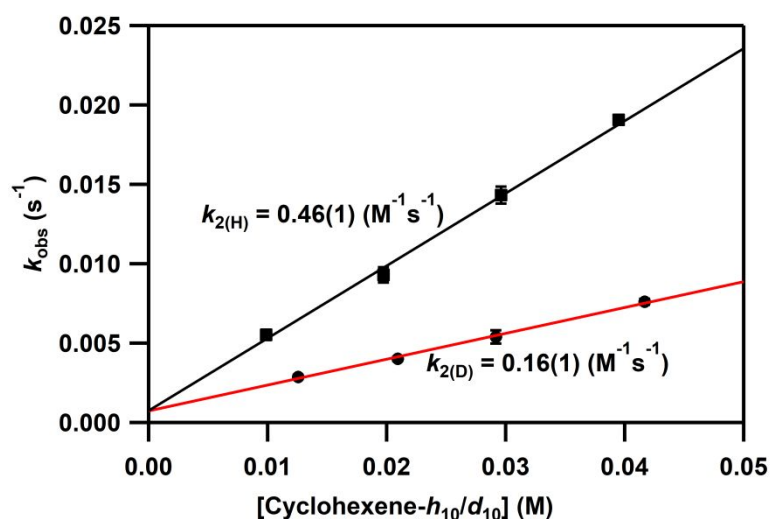
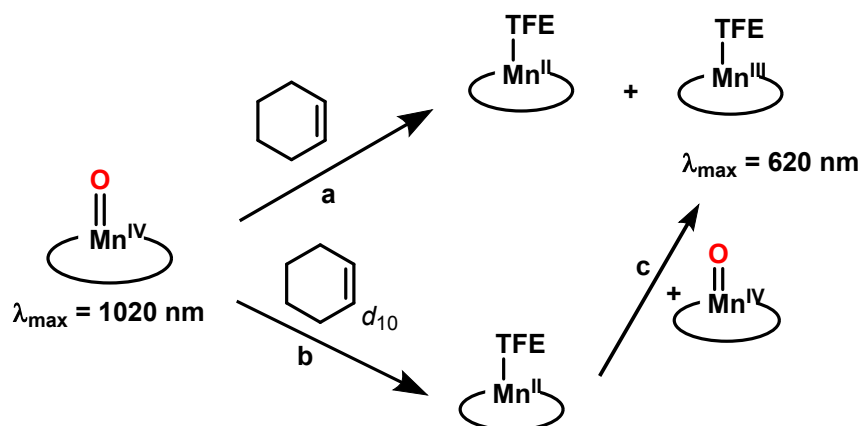


Figure 9. Plots of the pseudo-first-order rate constants (k_{obs}) against substrate concentration for the oxidation of cyclohexene (black squares) and cyclohexene- d_{10} (black circles) by $[\text{Mn}^{\text{IV}}(\text{O})(\text{N}2\text{py}2\text{Q})]^{2+}$ (**2**) in TFE (substrate dissolved in MeCN).



Scheme 2. Products formed in cyclohexene (a) and cyclohexene-*d*₁₀ (b) oxidation by Mn^{IV}-oxo adducts and competitive comproportionation reaction (c) in TFE at 298 K.

Reactivity of Mn^{IV}-oxo adducts with other olefins. The allylic C–H bond of cyclooctene has a stronger bond dissociation energy (83 kcal mol⁻¹) than cyclohexene (80 kcal mol⁻¹).⁴² To assess the effect of this change on the reactivity of **2-4** with olefins, we treated each complex with an excess of cyclooctene and monitored the reaction by electronic absorption spectroscopy. Addition of excess cyclooctene in CH₂Cl₂ (0.04–0.08 mM) to a solution of **2** in TFE at 298 K led to disappearance of the Mn^{IV}-oxo species following pseudo-first order kinetics (Figure 10, left). The variation in k_{obs} as a function of cyclooctene concentration yielded a second order rate constant (k_2) of $6.0 \times 10^{-1} \text{ M}^{-1} \text{ s}^{-1}$ (Figure 10, right). The spectral changes during this reaction do not provide evidence for the formation of a Mn^{III} product, indicating a two-electron epoxidation process resulting in formation of a Mn^{II} complex. This conclusion is bolstered by GC–MS product analysis, which confirms the formation of cyclooctene epoxide as the only detected product. The chromatogram obtained from GC did not show any peaks related to cyclooctenol or cyclooctenone. This observation is in line with the high BDE value of cyclooctene, which makes the allylic oxidation reaction slower than C=C epoxidation. The reaction kinetics of cyclooctene oxidation by **3** and **4** were too slow to obtain rates even with a high concentration of cyclooctene (0.8 M).

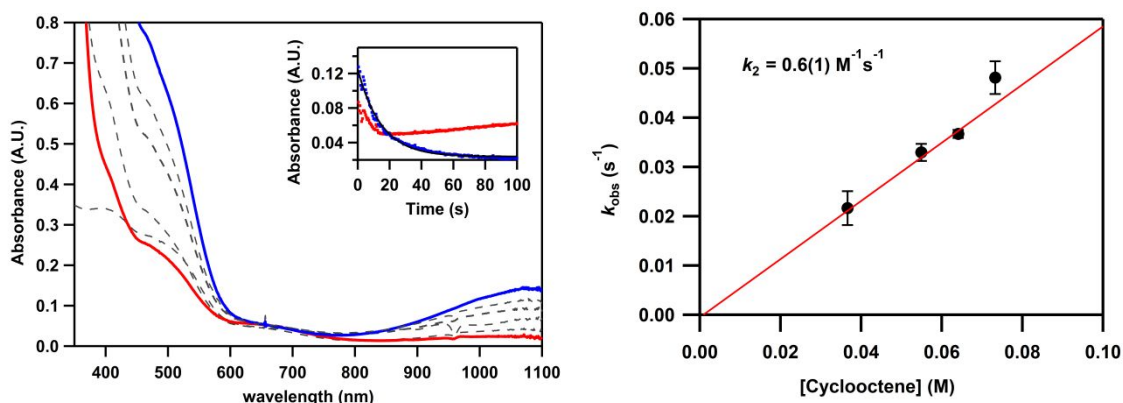


Figure 10. Left: Reaction of 1.0 mM $[\text{Mn}^{\text{IV}}(\text{O})(\text{N}2\text{py}2\text{Q})]^{2+}$ (**2**) with 80 equiv. cyclooctene in TFE. Inset: decay of the feature at 920 nm (blue trace) and the minimal growth of the feature at 620 nm (red trace). Right: Plot of the pseudo-first-order rate constants (k_{obs}) against substrate concentration for the reaction between $[\text{Mn}^{\text{IV}}(\text{O})(\text{N}2\text{py}2\text{Q})]^{2+}$ (**2**) and cyclooctene in TFE.

The reactivity of **2-4** with styrene was also investigated. Although styrene oxidation reactions by **3** and **4** were too sluggish to permit collection of rate data (even at 0.6 M), reactions of **2** with styrene were quite rapid. The addition of an excess of styrene (0.04–0.1 M) dissolved in CH_2Cl_2 to a solution of **2** in TFE lead to the disappearance of the Mn^{IV} -oxo band at 1020 nm (Figure 11, left). The second order rate constant of $7(1) \times 10^{-1} \text{ M}^{-1} \text{ s}^{-1}$ at 298 K was obtained for styrene oxidation by **2** from a linear relation between observed rate constant (k_{obs}) and increasing styrene concentration (Figure 11, right). This rate was found to be 1.5-fold faster than the oxidation rate of cyclohexene by **2**. The spectral changes during this reaction are similar to the reaction of **2** with cyclooctene, where there is a little growth of a band at 620 nm. Thus, we conclude a dominant Mn^{II} product. This observation is also supported by GC–MS product analysis, which shows the formation of styrene oxide as the sole detected product. Interestingly, the rate constant obtained with cyclooctene, and styrene are very similar to that obtained for cyclohexene oxidation by **2** under similar conditions (Table 1). A rate comparison for cyclooctene oxidation by **1** and **5** is summarized in Table 1, demonstrating that **2** shows rate enhancement of ~ 110 -fold and 18-fold relative to **1** and **5**. Thus, **2** is one of the most reactive Mn^{IV} -oxo centers for olefin epoxidation.

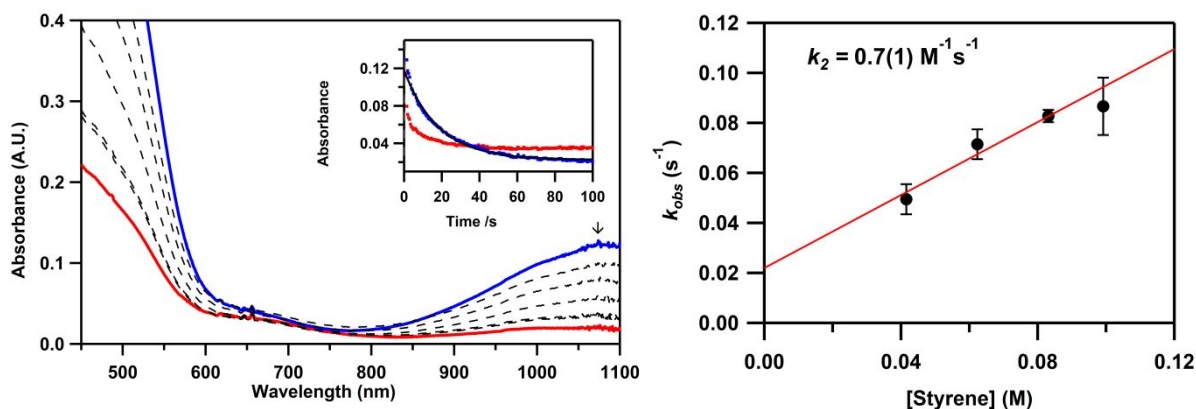


Figure 11. Left: Reaction of 1.0 mM $[\text{Mn}^{\text{IV}}(\text{O})(\text{N}2\text{py}2\text{Q})]^{2+}$ (**2**) with 45 equiv. of styrene in TFE. Inset: decay of the feature at 1020 nm (blue trace) over time and the minimal change observed at 620 nm (red trace). Right: Plot of the pseudo-first order rate constants (k_{obs}) against the concentration of styrene.

Understanding the chemoselectivity of Mn^{IV} -oxo complexes. In a previous study, we explored HAT reactions of complexes **1-4** with various hydrocarbons differing in C–H bond strength, which demonstrated a trend of increasing rates in the order $2 > 1 > 4 > 3$ (Figure S6).^{25a} On the other hand, when these complexes were investigated for sulfoxidation reactions with thioanisole, the reactivity trend changed to $2 \gg 1 > 3 > 4$ (Figure S7).^{25a} In this present study we have observed that the trend in olefin oxidation rates follows the same trend observed in sulfoxidation rates. Remarkably, even though **2** is capable of reacting with C–H bonds as strong as $99.9 \text{ kcal mol}^{-1}$ (cyclohexane),²⁶ the epoxide:allylic oxidation ratio for **2** shows a high preference for epoxidation that is unusual among Mn^{IV} -oxo complexes. Along the same lines, **3** also favors epoxidation over C–H bond oxidation. In this case the preference can be rationalized given that **3** shows fairly rapid OAT rates, whereas it is a sluggish oxidant for C–H bond oxidation (Figure S6 and S7). On the other hand, complexes **1** and **4** show a markedly different product selectivity, favoring allylic oxidation over epoxidation. These collective observations lead to the question – What causes the different trends in OAT and HAT rates for this set of similar Mn^{IV} -oxo complexes?

In a study by Nam *et al.*, Mn^{IV} -oxo complexes in the presence of Brønsted acids reacted with cyclohexene to exclusively form the epoxidation product, while the Mn^{IV} -oxo without acid preferred the HAT pathway forming allylic oxidation products.²² This change in chemoselectivity for the acid bound complexes was attributed to a change to a favorable electron transfer (ET) mechanism in substrate oxidation.⁴¹ This change in mechanisms is a direct consequence of a dramatic shift in potential for **1** (0.80 V to 1.65 V vs SCE) and **5** (0.78 V to 1.50 V vs SCE) in the presence of Brønsted acids. Very recently, our group provided evidence that **2-4** share the same direct oxygen atom transfer mechanism for

thioanisole sulfoxidation.²⁷ On this basis, and considering the fairly modest cathodic peak potentials for these Mn^{IV}-oxo complexes observed by cyclic voltammetry ($E_{p,c} = 0.47\text{--}1.01$ V vs SCE),^{25a} we presume that epoxidation of cyclohexene also occurs by a direct OAT mechanism. Therefore, the differences in chemoselectivity obtained in the current series are unlikely to be an outcome of a change in mechanism.

To provide insight into these unexplained differences in chemoselectivity, we performed DFT computations to understand the fundamental thermodynamics of the OAT and HAT processes for these Mn^{IV}-oxo complexes. Because HAT and OAT rates for series of metal-oxo complexes commonly follow linear-free energy relationships,^{25b, 27, 43} trends in reactions rates can be understood on the basis of differences in thermodynamic driving force. This approach also avoids the identification of transition states, which can be particularly challenging for Mn^{IV}-oxo complexes. For example, previous DFT calculations on HAT and OAT reactions of Mn^{IV}-oxo complexes have shown involvement of multiple electronic states, some of different spin multiplicity than the ground state, that cross along the reaction coordinate.⁴⁴ Moreover, DFT methods appear to underestimate transition-state energies for HAT reactions of Mn^{IV}-oxo complexes, with the CASSCF/NEVPT2 method providing a more rigorous approach.⁴⁵ Although these calculations predict the correct reactivity trend, they are laborious and still rely on transition-state geometries from DFT methods. In the DFT approach employed here, we found that the reactivity trends of Mn^{IV}-oxo systems can be readily explained using thermodynamic properties of products and reactants, which can be calculated in a straightforward fashion.

This approach was initially motivated by the DFT-computed geometric structures of **2** and **3**, which show a relatively large tilt in the axial bond angle involving the amine ligand (see Supporting Information, Figure S8), the Mn^{IV} center, and the oxo moiety (**2**: $\angle\text{O-Mn-N}_{\text{axial}} = 170.6^\circ$; **3**: $\angle\text{O-Mn-N}_{\text{axial}} = 177.5^\circ$ as compared to **4** $\angle\text{O-Mn-N}_{\text{axial}} = 178.8^\circ$).^{25a} We speculated that this tilt would slightly weaken π -overlap between the manganese and oxygen orbitals, potentially reducing the Mn=O bond dissociation free energy. To test this theory, we calculated Mn^{IV}=O BDFE values for **1-4** (Table 3). From these calculations, we find a range in Mn^{IV}=O BDFEs from 64.0 to 72.1 kcal mol⁻¹, with **2** and **4** having the weakest and strongest BDFEs, respectively. The weakest BDFE for **2** marks this complex as the best oxygen-atom donor of the series, and is consistent with this complex being the most rapid OAT agent in this series. Overall, we observe an increase in Mn^{IV}=O BDFEs of **2** < **1** \approx **3** < **4**, which nicely follows the trend in OAT rates for thioanisole oxidation by these complexes.

Indeed, a plot of $\log k_2$ for thioanisole oxidation versus $\text{Mn}^{\text{IV}}=\text{O}$ BDFE is linear (Figure 12, left), which supports our postulate that the differences in OAT reactions rates among this series has its basis in differences in $\text{Mn}^{\text{IV}}=\text{O}$ bond strength. Though a direct relationship between the $\text{N}_{\text{ax}}-\text{Mn}=\text{O}$ angle and the $\text{Mn}^{\text{IV}}-\text{oxo}$ BDFE is not observed (Table 3), a large deviation in this angle contributes to a reduction in the $\text{Mn}^{\text{IV}}-\text{oxo}$ BDFE. This angle dependence of the $\text{Mn}^{\text{IV}}=\text{O}$ BDFE was tested for **1** by varying the axial angle from 179.6° to 168.2° , which revealed a decrease in the $\text{Mn}=\text{O}$ bond strength by 3 kcal mol^{-1} (see Supporting Information, Figure S9). Thus, the slight $\text{N}_{\text{ax}}-\text{Mn}=\text{O}$ tilt in **2** and **3** likely serves to weaken the $\text{Mn}=\text{O}$ bond strength and is one of several parameters that influences the $\text{Mn}^{\text{IV}}=\text{O}$ BDFE.

Similarly, we calculated O–H BDFEs for Mn^{III} -hydroxo complexes, which are the products of HAT reactions of the $\text{Mn}^{\text{IV}}-\text{oxo}$ complexes. In this case, stronger O–H BDFEs should correlate with faster HAT reaction rates. Table 3 shows the ΔBDFE values for the O–H bonds of the Mn^{III} -hydroxo complexes relative to that of **1** (we consider ΔBDFE in this case because the protocol for calculating absolute BDFEs requires corrections due to solvent, which are not known for the experimental solvent TFE). From these calculations, we observe an ordering of **2** > **1** > **4** > **3**, which yields a linear relationship when plotted against $\log k_2$ for DHA oxidation by these complexes (Figure 12, right). Thus, the O–H BDFE in the Mn^{III} -hydroxo products is able to reproduce the HAT reaction rates. Moreover, these DFT calculations also reproduce the difference in ordering for the OAT and HAT reactions. While the $\text{Mn}^{\text{III}}\text{O}-\text{H}$ bond strength of **3** is weaker than **4**, consistent with poor reactivity for HAT reactions by **3**, the $\text{Mn}^{\text{IV}}=\text{O}$ bond strength of **3** is much weaker than that of **4**, making the former complex more adept at OAT reactions. When applied to cyclohexene oxidation, the coupling of the weak $\text{Mn}^{\text{IV}}=\text{O}$ bond and weak $\text{Mn}^{\text{III}}\text{O}-\text{H}$ bond of **3** lead to a favorable epoxidation reaction over allylic oxidation.

Table 3. DFT calculated bond dissociation free energies of $\text{Mn}^{\text{IV}}-\text{oxo}$ adducts in kcal mol^{-1} and tilt in the axial angle.

Complex	BDFE of $\text{Mn}^{\text{IV}}=\text{O}$	ΔBDFE		
		$\text{Mn}^{\text{IV}}=\text{O}$	$\text{Mn}^{\text{III}}\text{O}-\text{H}$	$\angle\text{O}-\text{Mn}-\text{N}_{\text{ax}}$
$[\text{Mn}^{\text{IV}}(\text{O})(\text{N}2\text{py}2\text{Q})]^{2+}$ (2)	64.0	-3.6	4.4	170.0
$[\text{Mn}^{\text{IV}}(\text{O})(\text{N}4\text{py})]^{2+}$ (1)	67.7	0.0	0.0	179.6
$[\text{Mn}^{\text{IV}}(\text{O})(\text{N}2\text{py}2\text{B})]^{2+}$ (3)	68.1	0.5	-2.7	177.2
$[\text{Mn}^{\text{IV}}(\text{O})(\text{DMMN}4\text{py})]^{2+}$ (4)	72.1	4.4	-1.6	178.8

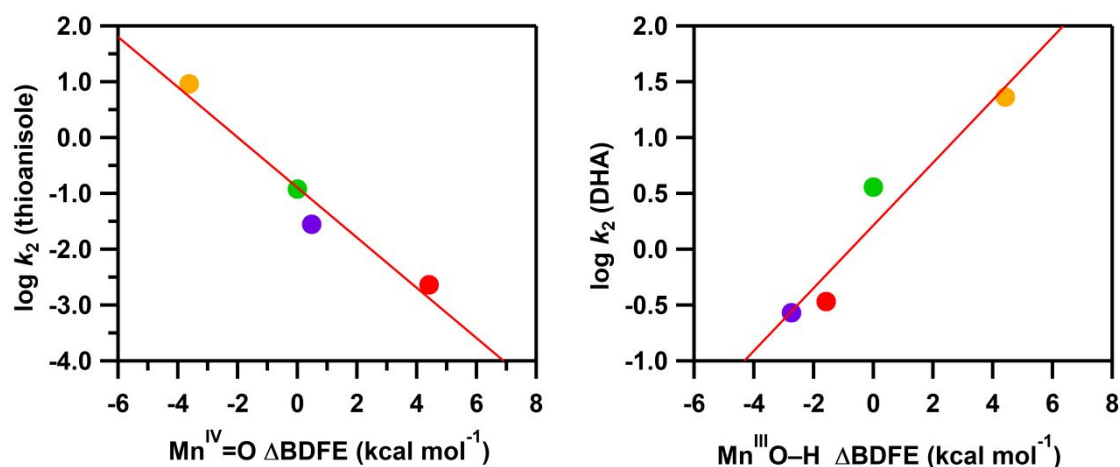


Figure 11. Correlation plot of calculated BDFE of $[\text{Mn}^{\text{IV}}(\text{O})(\text{N}4\text{py})]^{2+}$ (**1**, green circle), $[\text{Mn}^{\text{IV}}(\text{O})(\text{N}2\text{py}2\text{Q})]^{2+}$ (**2**, orange circle), $[\text{Mn}^{\text{IV}}(\text{O})(\text{N}2\text{py}2\text{B})]^{2+}$ (**3**, purple circle), $[\text{Mn}^{\text{IV}}(\text{O})(^{\text{DMM}}\text{N}4\text{py})]^{2+}$ (**4**, red circle) with experimental $\log(k_2)$ of thioanisole oxidation (left) and DHA oxidation (right) by Mn^{IV} -oxo adducts.

Conclusions

In this work, we have presented a comparative study of olefin oxidation reactions using a series of Mn^{IV} -oxo complexes supported by neutral pentadentate N_5 ligands with different steric and electronic properties. Our previous work with these complexes demonstrated large rate enhancements as a function of these simple changes in the equatorial ligand field for both HAT and OAT reactions.^{25a, 25b} Relatively, the rate variation in OAT reactions is larger among **2-4** than the rate variations observed in HAT reactions. Based on these results, we anticipated that Mn^{IV} -oxo complexes would show different selectivity for substrates susceptible to allylic C–H bond oxidation and olefin epoxidation. We examined this matter using cyclohexene and cyclooctene as probes. Interestingly, the strongest oxidant in the series, **2**, preferentially reacts with C=C bond of cyclohexene to give a 2:1 ratio of epoxide over allylic products. When cyclohexene was replaced with cyclohexene-*d*₁₀, cyclooctene, or styrene, C=C epoxidation becomes even more dominant over allylic C–H oxidation, yielding epoxides as the sole detected products. The cyclohexene-*d*₁₀ oxidation also reflects the true epoxidation rates of cyclohexene by **2** as oxidant. Although on the slower side of the reactivity spectrum, **3** has demonstrated faster kinetics in OAT reactions as compared to HAT.^{25a} This trend is reinforced in the current study where the reaction of **3** with cyclohexene results in a roughly 2:1 ratio of epoxidation product over allylic oxidation products. On the other hand, the electron rich Mn^{IV} -oxo center in **4** favors allylic oxidation,

yielding 35% and 12% of cyclohexenol and cyclohexenone over 21% of corresponding epoxide. The chemoselectivity observed in olefin oxidation using Mn^{IV}-oxo adducts **2-4** could be explained by weakening of the Mn=O bond, as demonstrated by DFT calculated Mn=O BDFEs. This distortion in the geometry of **2** and **3** is influenced by sterics introduced through bulky quinoline and benzimidazole substituents in the equatorial ligand field. The DFT computations used to obtain thermodynamic properties of the Mn^{IV}-oxo complexes were able to reproduce the reactivity trends in OAT and HAT reactions, allowing us to rationalize the change in chemoselectivity patterns of structurally similar Mn^{IV}-oxo complexes on the basis of straightforward thermodynamic parameters. We expect that such strategies could be fruitful in the rational design of transition-metal compounds for chemoselective substrate oxidation.

Author contribution.

P.S., M.C.D., J.R.M. and T.A.J conceived and planned the experiments. P.S. and M.C.D. performed all experiments. The computational calculations were performed by P.S. and J.R.M. All authors contributed to the data analysis and provided contribution in writing of the final manuscript.

Conflicts of Interest.

There are no conflicts to declare.

Acknowledgements.

This work was supported by the U.S. D.O.E. (DE-SC0016359). Support for the NMR instrumentation was provided by NIH Shared Instrumentation Grant # S10OD016360. J.R.M. was supported by the National Institutes of Health Graduate Training Program in Dynamic Aspects of Chemical Biology (Grant T32 GM1001147) and Graduate Training in Chemical Biology (T32 GM132061). We thank the Mass Spectrometry and Analytical Proteomics Laboratory, University of Kansas, KS and Dr. Anita Saraf and Lawrence Seib for their help with analytical method development, sample analysis, data interpretation.

References:

1. a) K. A. Joergensen, *Chem. Rev.*, 1989, **89**, 431-458; b) A. E. Shilov and G. B. Shul'pin, *Chem. Rev.*, 1997, **97**, 2879-2932; c) R. A. Sheldon and J. K. Kochi, in *Metal-catalyzed Oxidations of Organic Compounds*, eds. R. A. Sheldon and J. K.

- Kochi, Academic Press, 1981, DOI: <https://doi.org/10.1016/B978-0-12-639380-4.50007-5>, pp. 1-14.
2. a) M. Costas, A. K. Tipton, K. Chen, D.-H. Jo and L. Que, *J. Am. Chem. Soc.*, 2001, **123**, 6722-6723; b) K. Suzuki, P. D. Oldenburg and L. Que Jr., *Angew. Chem. Int. Ed.*, 2008, **47**, 1887-1889.
 3. a) S. Samanta, S. C. Laha, N. K. Mal and A. Bhaumik, *J. Mol. Catal. A Chem.*, 2004, **222**, 235-241; b) A. Nishinaga, K. Maruyama, T. Mashino, K. Yoda and H. Okamoto, in *Studies in Surface Science and Catalysis*, ed. L. I. Simándi, Elsevier, 1991, vol. 66, pp. 93-102.
 4. J. Muzart, *Chem. Rev.*, 1992, **92**, 113-140.
 5. a) J. W. de Boer, J. Brinksma, W. R. Browne, A. Meetsma, P. L. Alsters, R. Hage and B. L. Feringa, *J. Am. Chem. Soc.*, 2005, **127**, 7990-7991; b) I. Garcia-Bosch, A. Company, X. Fontrodona, X. Ribas and M. Costas, *Org. Lett.*, 2008, **10**, 2095-2098; c) G. Yin, A. M. Danby, D. Kitko, J. D. Carter, W. M. Scheper and D. H. Busch, *Inorg. Chem.*, 2007, **46**, 2173-2180; d) W. Zhang, J. L. Loebach, S. R. Wilson and E. N. Jacobsen, *J. Am. Chem. Soc.*, 1990, **112**, 2801-2803.
 6. a) Z. Lv, W. Zheng, Z. Chen, Z. Tang, W. Mo and G. Yin, *Dalton Trans.*, 2016, **45**, 11369-11383; b) T. K. M. Shing, E. K. W. Tam, V. W.-F. Tai, I. H. F. Chung and Q. Jiang, *Chem. Eur. J.*, 1996, **2**, 50-57.
 7. a) V. A. Likhoholov, in *Studies in Surface Science and Catalysis*, ed. L. I. Simándi, Elsevier, 1991, vol. 66, pp. 103-112; b) A. Wang and H. Jiang, *J. Org. Chem.*, 2010, **75**, 2321-2326.
 8. Y. Shen, P. Jiang, P. T. Wai, Q. Gu and W. Zhang, *Catalysts*, 2019, **9**, 31.
 9. D. Munz, D. Wang, M. M. Moyer, M. S. Webster-Gardiner, P. Kunal, D. Watts, B. G. Trewyn, A. N. Vedernikov and T. B. Gunnoe, *ACS Catal.*, 2016, **6**, 4584-4593.
 10. a) M. Sono, M. P. Roach, E. D. Coulter and J. H. Dawson, *Chem. Rev.*, 1996, **96**, 2841-2888; b) W. Zhu and N. G. J. Richards, *Essays Biochem.*, 2017, **61**, 259-270; c) E. I. Solomon, D. E. Heppner, E. M. Johnston, J. W. Ginsbach, J. Cirera, M. Qayyum, M. T. Kieber-Emmons, C. H. Kjaergaard, R. G. Hadt and L. Tian, *Chem. Rev.*, 2014, **114**, 3659-3853.

11. a) P. R. Ortiz de Montellano, *Chem. Rev.*, 2010, **110**, 932-948; b) E. G. Kovaleva and J. D. Lipscomb, *Nat. Chem. Biol.*, 2008, **4**, 186-193; c) M. Balamurugan, N. Saravanan, H. Ha, Y. H. Lee and K. T. Nam, *Nano Converg.*, 2018, **5**, 18; d) A. D. N. Vaz, D. F. McGinnessy and M. J. Coon, *Proc. Nat. Acad. Sci.*, 1998, **95**, 3555.
12. a) R. Iwanejko, P. Leduc, T. Mlodnicka and J. Poltowicz, in *Studies in Surface Science and Catalysis*, ed. L. I. Simándi, Elsevier, 1991, vol. 66, pp. 113-120; b) N. Suzuki, T. Higuchi, Y. Urano, K. Kikuchi, H. Uekusa, Y. Ohashi, T. Uchida, T. Kitagawa and T. Nagano, *J. Am. Chem. Soc.*, 1999, **121**, 11571-11572; c) A. Takahashi, T. Kurahashi and H. Fujii, *Inorg. Chem.*, 2007, **46**, 6227-6229; d) M. Guo, T. Corona, K. Ray and W. Nam, *ACS Cent. Sci.*, 2019, **5**, 13-28.
13. a) I. Ojima, *Catalytic asymmetric synthesis*, John Wiley & Sons, 2010; b) K. Srinivasan, P. Michaud and J. K. Kochi, *J. Am. Chem. Soc.*, 1986, **108**, 2309-2320; c) A. L. I. Allahresani and M. A. Nasser, *J. Chem. Sci.*, 2017, **129**, 343-352.
14. a) M. M. Pereira, L. D. Dias and M. J. F. Calvete, *ACS Catal.*, 2018, **8**, 10784-10808; b) R. Gupta, X.-X. Li, K.-B. Cho, M. Guo, Y.-M. Lee, Y. Wang, S. Fukuzumi and W. Nam, *J. Phys. Chem. Lett.*, 2017, **8**, 1557-1561.
15. a) L. Vicens, G. Olivo and M. Costas, *ACS Catal.*, 2020, **10**, 8611-8631; b) B. Wang, Y.-M. Lee, M. S. Seo and W. Nam, *Angew. Chem. Int. Ed.*, 2015, **54**, 11740-11744.
16. K. Chen and L. Que, *J. Am. Chem. Soc.*, 2001, **123**, 6327-6337.
17. R. E. White and M. J. Coon, *Ann. Rev. Biochem.*, 1980, **49**, 315-356.
18. a) J. Du, C. Miao, C. Xia, Y.-M. Lee, W. Nam and W. Sun, *ACS Catal.*, 2018, **8**, 4528-4538; b) R. V. Ottenbacher, D. G. Samsonenko, E. P. Talsi and K. P. Bryliakov, *ACS Catal.*, 2016, **6**, 979-988; c) D. Shen, C. Saracini, Y.-M. Lee, W. Sun, S. Fukuzumi and W. Nam, *J. Am. Chem. Soc.*, 2016, **138**, 15857-15860; d) S. P. de Visser, F. Ogliaro, P. K. Sharma and S. Shaik, *J. Am. Chem. Soc.*, 2002, **124**, 11809-11826; e) S. Shaik, S. P. de Visser and D. Kumar, *J. Am. Chem. Soc.*, 2004, **126**, 11746-11749.
19. W. N. Oloo, Y. Feng, S. Iyer, S. Parmelee, G. Xue and L. Que, *New J. Chem.*, 2013, **37**, 3411-3415.
20. S. N. Dhuri, K.-B. Cho, Y.-M. Lee, S. Y. Shin, J. H. Kim, D. Mandal, S. Shaik and W. Nam, *J. Am. Chem. Soc.*, 2015, **137**, 8623-8632.

21. Y. H. Kwon, B. K. Mai, Y.-M. Lee, S. N. Dhuri, D. Mandal, K.-B. Cho, Y. Kim, S. Shaik and W. Nam, *J. Phys. Chem. Lett.*, 2015, **6**, 1472-1476.
22. S. Kim, K.-B. Cho, Y.-M. Lee, J. Chen, S. Fukuzumi and W. Nam, *J. Am. Chem. Soc.*, 2016, **138**, 10654-10663.
23. a) C. Miao, B. Wang, Y. Wang, C. Xia, Y.-M. Lee, W. Nam and W. Sun, *J. Am. Chem. Soc.*, 2016, **138**, 936-943; b) C. Choe, L. Yang, Z. Lv, W. Mo, Z. Chen, G. Li and G. Yin, *Dalton Trans.*, 2015, **44**, 9182-9192.
24. J. F. Bartoli, O. Brigaud, P. Battioni and D. Mansuy, *J. Chem. Soc., Chem. Commun.*, 1991, DOI: 10.1039/C39910000440, 440-442.
25. a) M. C. Denler, A. A. Massie, R. Singh, E. Stewart-Jones, A. Sinha, V. W. Day, E. Nordlander and T. A. Jackson, *Dalton Trans.*, 2019, **48**, 5007-5021; b) A. A. Massie, M. C. Denler, L. T. Cardoso, A. N. Walker, M. K. Hossain, V. W. Day, E. Nordlander and T. A. Jackson, *Angew. Chem. Int. Ed.*, 2017, **56**, 4178-4182; c) A. A. Massie, M. C. Denler, R. Singh, A. Sinha, E. Nordlander and T. A. Jackson, *Chem. –Eur. J.*, 2020, **26**, 900-912.
26. A. A. Massie, A. Sinha, J. D. Parham, E. Nordlander and T. A. Jackson, *Inorg. Chem.*, 2018, **57**, 8253-8263.
27. P. Singh, E. Stewart-Jones, M. C. Denler and T. A. Jackson, *Dalton Trans.*, 2021, **50**, 3577-3585.
28. J. G. S. a. H. Saltzman, *Org. synth.*, 1963, **43**, 65.
29. a) W. K. C. Lo, C. J. McAdam, A. G. Blackman, J. D. Crowley and D. A. McMorran, *Inorganica Chim. Acta*, 2015, **426**, 183-194; b) M. Lubben, A. Meetsma, E. C. Wilkinson, B. Feringa and L. Que Jr, *Angew. Chem. Int. Ed.*, 1995, **34**, 1512-1514; c) M. Mitra, H. Nimir, S. Demeshko, S. S. Bhat, S. O. Malinkin, M. Haukka, J. Lloret-Fillol, G. C. Lisensky, F. Meyer, A. A. Shteinman, W. R. Browne, D. A. Hrovat, M. G. Richmond, M. Costas and E. Nordlander, *Inorg. Chem.*, 2015, **54**, 7152-7164; d) S. Rana, A. Dey and D. Maiti, *Chem. Commun.*, 2015, **51**, 14469-14472.
30. A. Durazo and M. M. Abu-Omar, *Chem. Commun.*, 2002, DOI: 10.1039/B108864E, 66-67.
31. F. Neese, *WIREs Comput. Mol. Sci.*, 2012, **2**, 73-78.

32. a) C. Lee, W. Yang and R. G. Parr, *Phys. Rev. B*, 1988, **37**, 785-789; b) A. D. Becke, *J. Chem. Phys.*, 1993, **98**, 5648-5652.
33. S. Grimme, J. Antony, S. Ehrlich and H. Krieg, *J. Chem. Phys.*, 2010, **132**, 154104.
34. S. Grimme, S. Ehrlich and L. Goerigk, *J. Comput. Chem.*, 2011, **32**, 1456-1465.
35. a) F. Weigend, *Phys. Chem. Chem. Phys.*, 2006, **8**, 1057-1065; b) F. Weigend and R. Ahlrichs, *Phys. Chem. Chem. Phys.*, 2005, **7**, 3297-3305.
36. G. L. Stoychev, A. A. Auer and F. Neese, *J. Chem. Theory Comput.*, 2017, **13**, 554-562.
37. A. V. Marenich, C. J. Cramer and D. G. Truhlar, *J. Phys. Chem. B*, 2009, **113**, 6378-6396.
38. J. M. Mayer, in *Biomimetic Oxidations Catalyzed by Transition Metal Complexes*, DOI: 10.1142/9781848160699_0001, pp. 1-43.
39. a) D. F. Leto, R. Ingram, V. W. Day and T. A. Jackson, *Chem. Commun.*, 2013, **49**, 5378-5380; b) K.-B. Cho, H. Hirao, S. Shaik and W. Nam, *Chem. Soc. Rev.*, 2016, **45**, 1197-1210.
40. However, it was found that **2** reacts with 200 μL of MeCN with a rate constant of $1.97(3) \times 10^{-3} \text{ s}^{-1}$ (Figure S2), but this rate is 2.5-fold slower than the reaction of **2** with lowest concentration (10 equiv.) of cyclohexene employed ($k_{10 \text{ equiv.}} = 4.98 \times 10^{-3} \text{ s}^{-1}$) in the kinetic studies. Furthermore, we confirmed that the reaction between **2** and MeCN does not complicate the kinetic profile of cyclohexene oxidation by performing the same reaction with cyclohexene dissolved in CH_2Cl_2 . This set of reactions yielded a k_2 of $5.2(3) \times 10^{-1} \text{ M}^{-1} \text{ s}^{-1}$ (Figure S1), which is nearly identical to the k_2 determined with cyclohexene dissolved in MeCN.
41. Y.-M. Lee, S. Kim, K. Ohkubo, K.-H. Kim, W. Nam and S. Fukuzumi, *J. Am. Chem. Soc.*, 2019, **141**, 2614-2622.
42. J. J. Warren, T. A. Tronic and J. M. Mayer, *Chem. Rev.*, 2010, **110**, 6961-7001.
43. J. Chen, H. Yoon, Y.-M. Lee, M. S. Seo, R. Sarangi, S. Fukuzumi and W. Nam, *Chem. Sci.*, 2015, **6**, 3624-3632.

44. a) K.-B. Cho, S. Shaik and W. Nam, *J. Phys. Chem. Lett.*, 2012, **3**, 2851-2856; b) J. Chen, K.-B. Cho, Y.-M. Lee, Y. H. Kwon and W. Nam, *Chem. Commun.*, 2015, **51**, 13094-13097.
45. D. B. Rice, A. A. Massie and T. A. Jackson, *Inorg. Chem.*, 2019, **58**, 13902-13916.